



Automatic prediction of tongue muscle activations using a finite element model

Ian Stavness^{a,c,*}, John E. Lloyd^b, Sidney Fels^b

^a Department of Bioengineering, Clark Center, Room S221, Stanford University, Mail Code 5448, 318 Campus Drive, Stanford, CA 94305, USA

^b Department of Electrical and Computer Engineering, University of British Columbia, Canada

^c Department of Computer Science, University of Saskatchewan, 110 Science Place, Saskatoon, SK S7N 5C9 Canada, Canada

ARTICLE INFO

Article history:

Accepted 22 August 2012

Keywords:

Tongue
Muscle function
Finite-element methods
Forward-dynamics tracking simulation
Muscular-hydrostat modeling

ABSTRACT

Computational modeling has improved our understanding of how muscle forces are coordinated to generate movement in musculoskeletal systems. Muscular-hydrostat systems, such as the human tongue, involve very different biomechanics than musculoskeletal systems, and modeling efforts to date have been limited by the high computational complexity of representing continuum-mechanics. In this study, we developed a computationally efficient tracking-based algorithm for prediction of muscle activations during dynamic 3D finite element simulations. The formulation uses a local quadratic-programming problem at each simulation time-step to find a set of muscle activations that generated target deformations and movements in finite element muscular-hydrostat models. We applied the technique to a 3D finite element tongue model for protrusive and bending movements. Predicted muscle activations were consistent with experimental recordings of tongue strain and electromyography. Upward tongue bending was achieved by recruitment of the superior longitudinal sheath muscle, which is consistent with muscular-hydrostat theory. Lateral tongue bending, however, required recruitment of contralateral transverse and vertical muscles in addition to the ipsilateral margins of the superior longitudinal muscle, which is a new proposition for tongue muscle coordination. Our simulation framework provides a new computational tool for systematic analysis of muscle forces in continuum-mechanics models that is complementary to experimental data and shows promise for eliciting a deeper understanding of human tongue function.

© 2012 Elsevier Ltd. All rights reserved.

1. Introduction

Muscular-hydrostats are complex biomechanical systems found in nature as tongues, tentacles, and trunks. These solely muscular organs are biomechanically distinct because they generate deformation, articulation, and movement without the mechanical support of a rigid skeletal structure (Kier and Smith, 1985). Instead, mechanical support is thought to be achieved by the incompressible nature of muscle tissue, as well as synergistic activation of orthogonally oriented muscle fibers (Gilbert et al., 2007). Muscular-hydrostats share common architectural features for which a biomechanical explanation has been posited: longitudinal muscle fibers are arranged at the peripheral margins of the organ to create bending movements through unilateral recruitment (see Kier and Smith, 1985, Fig. 7), and muscle fibers are arranged perpendicular to the

longitudinal direction (either transverse, vertical, radial or circular) to create longitudinal elongation by reducing the transverse cross-sectional area of the organ (see Kier and Smith, 1985, Fig. 5). While muscle architecture appears linked to biomechanics in muscular-hydrostat systems, the way in which muscle forces are coordinated to control movement and shape deformation remains unclear.

Computational modeling has been widely used to analyze musculo-skeletal biomechanics; however, modeling muscular-hydrostat systems entails a number of specific challenges as compared to musculoskeletal systems. Musculoskeletal models typically represent muscles as massless springs and neglect the effects of soft-tissues (Pai, 2010), whereas muscular-hydrostat models require a continuum mechanics approach to represent soft-tissue deformations. Finite-element (FE) methods are commonly used to represent the large number of degrees-of-freedom associated muscular-hydrostat movements, including bending, twisting, grooving, elongating, and shortening.

A number of macro-scale FE models have been developed to simulate 3D deformations of tentacles (Yekutieli et al., 2005; Liang et al., 2006) and tongues (Wilhelms-Tricarico, 1995; Buchaillard

* Corresponding author. Tel.: +1 306 966 7995; fax: +1 306 966 4884.

E-mail addresses: stavness@gmail.com (I. Stavness),

lloyd@cs.ubc.ca (J.E. Lloyd), ssfels@ece.ubc.ca (S. Fels).

URL: <http://www.cs.usask.ca/faculty/stavness> (I. Stavness).

et al., 2009; Fang et al., 2009; Wang et al., 2011; Stavness et al., 2011). Previously reported muscular-hydrostat models are commonly based on idealized morphology, however Mijailovich et al. (2010) developed a highly detailed 2D mid-sagittal model of the tongue derived directly from myofiber tracts measured with DTI. Mijailovich et al. used an inverse technique to predict muscle activations during swallowing, however, the majority of previous FE muscular-hydrostat models rely on manually tuned muscle activations to generate biomechanical simulations.

For musculoskeletal systems, inverse simulation techniques, such as *forward-dynamics tracking simulation* (see Erdemir et al., 2007, for review), have been applied to automatically predict muscle forces for prescribed kinematics, including lower limb (Thelen and Anderson, 2006; Hamner et al., 2010), hand (Sueda et al., 2008), and face (Sifakis et al., 2005) movements. Little work has been reported for inverse simulation methods applicable to FE models. Inverse methods are particularly useful for models of high complexity, such as muscular-hydrostats, where the relationship between force and movement is not readily apparent from inspection and manual tuning of muscle activations is tedious if not impossible. Forward-dynamics tracking simulation is a promising inverse approach because the target movement can be specified in a sub-set of the degrees-of-freedom, and the system dynamics are used to *fill in* the other unknown/unconstrained kinematics. To the best of our knowledge, forward-dynamics tracking simulation has not previously been used to analyze biomechanical systems without skeletal support.

The purpose of this study was to uncover the coordination of muscle forces during muscular-hydrostat movement using forward-dynamics tracking simulation. We developed a tracking controller for FE muscle models and used it to predict muscle forces for hydrostatic tongue movements, including anterior protrusion, upward bending, and lateral bending. We hypothesized that contralateral transverse and vertical muscle recruitment would contribute to lateral bending in addition to lateral longitudinal muscle recruitment described by Kier and Smith (1985). Moreover, we expected that the muscle activations predicted by our inverse simulations would be consistent with electromyographic recordings for tongue protrusion (Pittman and Bailey, 2009) and tissue strains measured by tagged Magnetic Resonance Imaging (MRI) for tongue bending (Napadow et al., 1999).

2. Methods

We developed a tracking-based inverse controller for FE muscle models and compared tongue muscle forces predicted by the controller to published data for number of putative tongue movements. The tongue model and controller were implemented in the ArtiSynth biomechanical modeling toolkit (University of British Columbia, Vancouver, Canada, www.artisynth.org). For a detailed description of the ArtiSynth forward-dynamics and FE simulation framework see Lloyd et al. (2012).

2.1. Inverse simulation framework

We formulated a tracking-based inverse controller, similar to the “Computed Muscle Control” algorithm (Thelen and Anderson, 2006) that is generally applicable to both FE and rigid-body biomechanical models. The controller solves a local optimization problem at each time step of a forward-dynamics simulation in order to find a set of muscle activations that drive a biomechanical model through a target movement trajectory.

Forward-dynamics simulation involves solving for the motion that results from applied forces, using Newton’s second law

$$M\ddot{\mathbf{u}} = \mathbf{f}(\mathbf{q}, \mathbf{u}, t), \tag{1}$$

where \mathbf{M} is the system’s composite mass matrix, \mathbf{f} , \mathbf{q} , and \mathbf{u} are the composite generalized forces, positions, and velocities, and t is time. Modeling muscular-hydrostats with FE results in a *stiff* mechanical system, and so (1) was integrated using a semi-implicit integrator. We also considered mechanical

systems with bilateral constraints,¹ such as joints and FE incompressibility, leading to the following linear system for determining the velocities \mathbf{u}^{k+1} at the next time step

$$\begin{pmatrix} \hat{\mathbf{M}} & -\mathbf{G}^T \\ \mathbf{G} & 0 \end{pmatrix} \begin{pmatrix} \mathbf{u}^{k+1} \\ \boldsymbol{\lambda} \end{pmatrix} = \begin{pmatrix} \mathbf{M}\mathbf{u}^k + h\hat{\mathbf{f}} \\ \mathbf{g} \end{pmatrix}. \tag{2}$$

Here $\hat{\mathbf{M}}$ and $\hat{\mathbf{f}}$ are the mass matrix and force vector augmented with force derivative terms, \mathbf{u}^k denotes the previous velocities, h is the step size, \mathbf{G} is a matrix of bilateral constraints, $\boldsymbol{\lambda}$ are the impulses that enforce the constraints, and \mathbf{g} is a term arising from $\hat{\mathbf{G}}$.

The inverse controller determined muscle activations at each integration time step using a quadratic program that minimized the tracking errors for a target movement trajectory while resolving muscle redundancy. For this purpose, the mechanical system forces were divided into *passive* and *active* components, so that

$$\mathbf{f} = \mathbf{f}_p(\mathbf{q}, \mathbf{u}, t) + \mathbf{f}_a(\mathbf{q}, \mathbf{u}, \mathbf{a}, t),$$

where \mathbf{a} is a vector of muscle activations, $\mathbf{a} = (a_0 \ a_1 \ \dots \ a_m)^T$, and each activation is bounded, $0 \leq a_i \leq 1$. For Hill-type muscle models, which are commonly used in biomechanical models, the activation $a_i(t)$ denotes the fraction of isometric force at time t to the maximum active force that can be generated by a muscle fiber at its instantaneous length and velocity (Zajac, 1989). Therefore, the active muscle force is locally linear with respect to activation, so that

$$\mathbf{f}_a = \mathbf{A}(\mathbf{q}, \mathbf{u})\mathbf{a}, \tag{3}$$

where \mathbf{A} is a matrix that maps muscle activations to the applied system forces. The \mathbf{A} matrix captures the force-length and force-velocity behavior of Hill-type muscle models, as well as how muscle forces are spatially distributed and applied to the mechanical system.

The movement target was specified by a target velocity \mathbf{v}_* defined in a sub-space of the total system velocities. The target velocity sub-space \mathbf{v} was related to the system velocities \mathbf{u} via a Jacobian matrix \mathbf{J}_m , so that $\mathbf{v} = \mathbf{J}_m\mathbf{u}$. For time step $k+1$, it is easy to see from (2) that \mathbf{u}^{k+1} is linear with respect to \mathbf{a} , so that

$$\mathbf{u}^{k+1} = \mathbf{u}_0 + \mathbf{H}_m\mathbf{a},$$

where \mathbf{u}_0 is the solution of \mathbf{u}^{k+1} for (2) with \mathbf{a} set to zero, and each column j of \mathbf{H}_m is the solution of \mathbf{u}^{k+1} for (2) with a right hand side of

$$\begin{pmatrix} \mathbf{A}^k \mathbf{e}_j \\ 0 \end{pmatrix},$$

with \mathbf{e}_j denoting the elementary unit vector with the j th element equal to one and other elements zero. We minimized the velocity tracking error $\|\mathbf{v}_* - \mathbf{J}_m\mathbf{u}^{k+1}\|$, which can be expressed in quadratic form as

$$\phi_m(\mathbf{a}) \equiv \frac{1}{2} \|\bar{\mathbf{v}} - \mathbf{H}_m\mathbf{a}\|^2,$$

with

$$\bar{\mathbf{v}} \equiv \mathbf{v}_* - \mathbf{J}_m\mathbf{u}_0 \quad \text{and} \quad \mathbf{H}_m \equiv \mathbf{J}_m\mathbf{H}_u.$$

Muscle redundancy makes it possible for multiple different muscle activation patterns to give rise to the same observed movement. To resolve muscle redundancy in our controller, we included an l^2 -norm regularization term, $\frac{1}{2}\mathbf{a}^T\mathbf{a}$, which has shown to be effective in tracking-based inverse simulations of gait with data from healthy subjects (Hamner et al., 2010). Combining the movement target, regularization, and muscle activations bounds, along with appropriate weighting terms, we constructed the following quadratic program:

$$\begin{aligned} \min_{\mathbf{a}} \quad & w_m\phi_m(\mathbf{a}) + \frac{w_a}{2}\mathbf{a}^T\mathbf{a}, \\ \text{subject to} \quad & 0 \leq \mathbf{a} \leq 1, \end{aligned} \tag{4}$$

where w_m and w_a are weights used to trade-off between cost terms.

The optimization program (4) was solved to find activations before each forward-dynamics time step. The ArtiSynth system solver was used to compute $\bar{\mathbf{v}}$ and \mathbf{H}_m , which took the majority of the computational time. The resulting quadratic program was dense but small since its dimension was the size of \mathbf{a} , i.e. the number of activations solved for.

2.2. Tongue model

The human tongue has a complex arrangement of muscle fibers, with intrinsic muscle groups located within the tongue body at approximately orthogonal orientations and extrinsic muscle groups originating from surrounding bony structures in the oral cavity and inserting into the tongue body. In order to capture this complexity, we have developed an anatomically representative 3D FE tongue model, as pictured in

¹ Unilateral constraints (such as contact) leads to a more complex mathematical programming problem with complementarity constraints (MPCC).

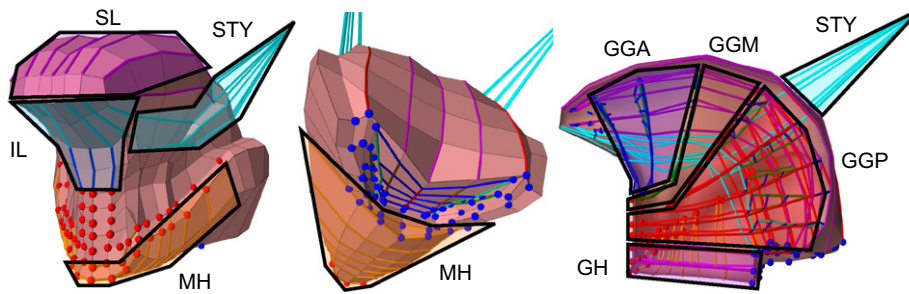
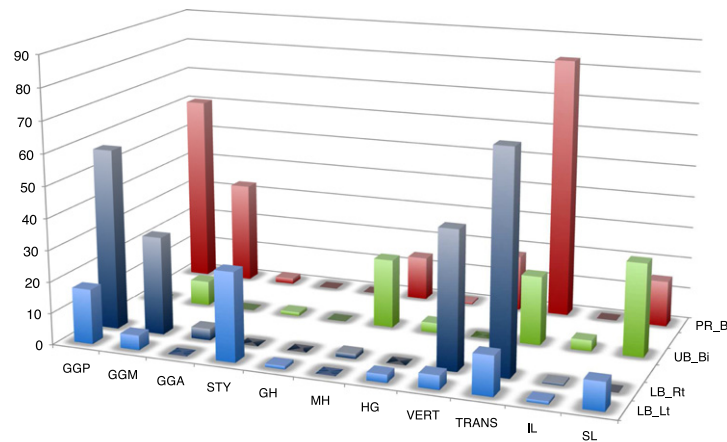


Fig. 1. Front, back, and sagittal cutaway views of tongue model. Attachment nodes are also shown for the jaw (front view, red spheres) and the hyoid bone (back view, blue spheres). Muscle groups are outlined with black lines and include the genioglossus (GGA, blue; GGM, brown; GGP, red), styloglossus (STY, cyan), geniohyoid (GH, magenta), mylohyoid (MH, orange), hyoglossus, (HG, red), vertical (VERT, green), transverse (TRANS, blue), inferior longitudinal (IL, cyan), and superior longitudinal (SL, magenta) muscles. (For interpretation of the references to color in this figure caption, the reader is referred to the web version of this article.)



Tongue Muscle Activations (%)											
GGP	GGM	GGA	STY	GH	MH	HG	VERT	TRANS	IL	SL	
60.3	32.6	1.8	0.0	0.0	13.9	0.5	17.7	82.8	0.0	14.6	PR_Bi
0.0	8.0	0.0	1.1	0.0	22.0	3.1	0.0	21.8	3.4	29.5	UB_Bi
17.5	4.6	0.0	28.3	1.0	0.0	2.5	4.4	12.4	0.9	8.8	LB_Lt
57.5	31.3	3.6	0.0	0.0	1.5	0.0	43.5	69.2	0.5	0.0	LB_Rt

Fig. 2. Predicted peak muscle activations (%) for simulated tongue movements: bilateral activations for protrusion (PR_Bi), bilateral activations for upward bending (UB_Bi), left-side activations for left-lateral bending (LB_Lt), and right-side activations for left-lateral bending (LB_Rt).

Fig. 1. The model was based on a reference model published by Buchaillard et al. (2009) and has been described in detail elsewhere (Stavness et al., 2011). It included 740 hexahedral elements (2493 degrees-of-freedom) with fixed boundary conditions for the muscle attachment sites on the mandible and hyoid bone. In order to simulate hydrostatic effects, we implemented tissue incompressibility using a constraint based mixed u–P formulation. We used hexahedral elements because incompressibility constraints with tetrahedral meshes can lead to artificial stiffening due to volumetric locking (Hughes, 2000).

Published values for the mechanical properties of tongue tissue vary widely in the literature (Cheng et al., 2011b). We chose material properties consistent with the reference model by Buchaillard et al. (2009): a fifth order incompressible Mooney–Rivlin material with $c_{10} = 1037$, $c_{20} = 486$, and $c_{01} = c_{11} = c_{02} = 0$ Pa, density of 1040 kg/m^3 , and Rayleigh damping coefficients of $\alpha = 40 \text{ s}^{-1}$ and $\beta = 0.03$. The Mooney–Rivlin material parameters were derived from ex vivo tongue tissue measurements (Gerard et al., 2005) and scaled by a factor of 5.4 in order to better match the in vivo Young’s modulus of skeletal muscle at rest (see Section 2B, Buchaillard et al., 2009). The shear modulus of the material at rest is 2.04 kPa , which is similar to the mean shear modulus of 2.67 kPa that was measured by MR elastography (Cheng et al., 2011b).

Muscle mechanics were implemented with 1574 Hill-type muscle fiber elements distributed throughout the FE mesh and spatially organized into 21

canonical muscle groups (depicted as colored lines in Fig. 1). We used the active force-length curve from the along-fiber stress term in Blemker et al. (2005). The maximum active isometric force of each muscle group was based on its maximum physiological cross-sectional area (see Table 1 in Buchaillard et al., 2009) assuming a muscle specific tension of 22 N/cm^2 . The instantaneous active muscle fiber force was scaled by activation, as described by Eq. (3) above. Our present study only examined slow speed tongue movements, therefore we neglected excitation dynamics (the time delay from muscle excitation to muscle activation), as well as force-velocity effects in the Hill-type model.

2.3. Target movements

We simulated three putative tongue movements: anterior protrusion, upward bending, and lateral bending. Target position trajectories for fourteen nodes on the anterior surface of the tongue model were smoothly interpolated between the rest and deformed positions. Target velocities were calculated by central differencing.

Simulations were performed on a 2.2 GHz Intel Core i7 processor. On average, each 10 ms forward-dynamics step took 104 ± 8 ms to compute. The inverse controller solve at each step took 386 ± 5 ms for protrusion and upward bending simulations (with 11 bilateral activations) and 643 ± 8 ms for lateral bending simulation (with 22 unilateral activations).

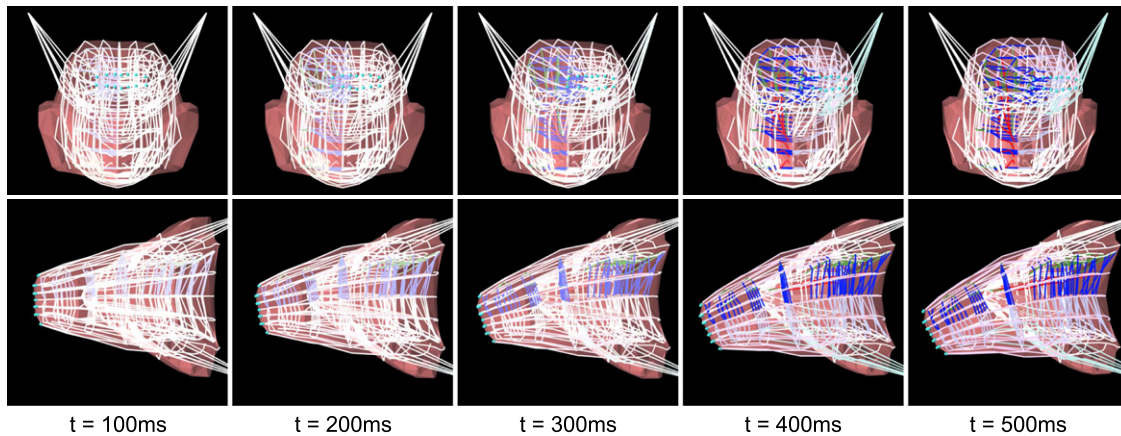


Fig. 3. A sequence of video frames showing predicted muscle activations (colored lines) and resulting movements with the 3D finite-element tongue model. (For interpretation of the references to color in this figure caption, the reader is referred to the web version of this article.)

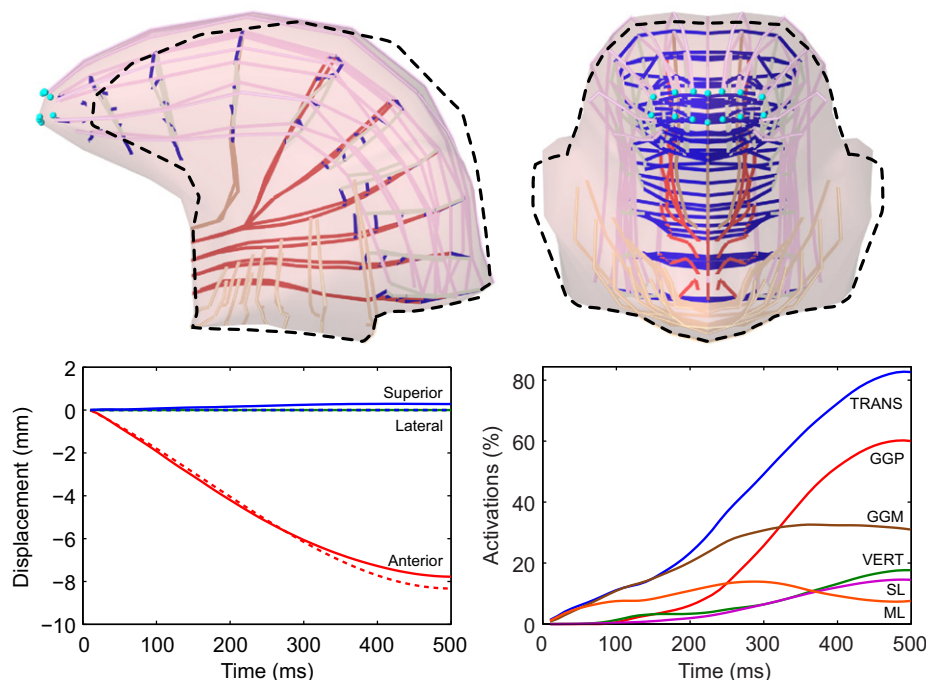


Fig. 4. Lateral and frontal views of the tongue model in the final protruded posture (upper-panels; black dashed lines denote rest posture). Plots show the position trajectory of tongue tip (lower-left panel; dashed lines denote target trajectory) and the predicted muscle activations for simulated protrusion (lower-right panel).

3. Results

A video of the resulting tongue simulations is shown in multimedia Fig. 3 and is available online at www.artisynth.org/inverse/tongue.mov. Predicted maximum muscle activation levels for each simulation are summarized in Fig. 2. For all simulations, tracking errors were small, but not zero, which was expected since the target movements were defined as a rigid movement of the tongue tip while the simulated movements required deformation of the tongue.

Anterior protrusion (Fig. 4) was achieved by synergistic bilateral activation of genioglossus and intrinsic (transverse and vertical) muscles. The superior longitudinal muscle was also activated to counteract the downward pull of the anterior part of the genioglossus muscle. The mylohyoid muscle was activated to stiffen and raise the floor of the mouth.

Upward bending (Fig. 5) was primarily achieved by superior longitudinal muscle activation. Bilateral transverse and mylohyoid muscles were also activated to stiffen the tongue body and stiffen

and raise the floor of the mouth. Middle genioglossus was activated to depress the middle tongue dorsum. (Which is observed during retroflex tongue postures, such as in the production of an English/r/sound.)

Left lateral bending (Fig. 6) was primarily achieved by unilateral activation of the contralateral (right-side) genioglossus and intrinsic (transverse and vertical) muscles, which elongated the right side of the tongue. Unilateral (left-side) styloglossus, superior longitudinal, and hyoglossus muscles were also activated to compress and retract the left-side of the tongue.

4. Discussion

4.1. Model limitations

The resolution of the current FE tongue model is coarse, which was a design decision to reduce the computational cost of

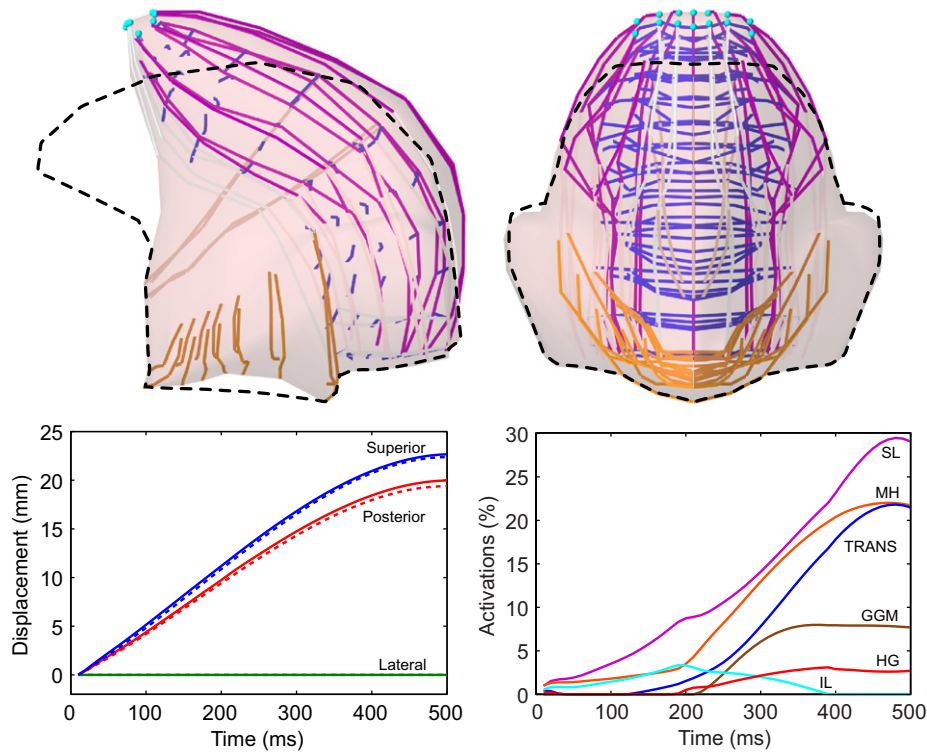


Fig. 5. Lateral and frontal views of the tongue model in the final upwardly bended posture (upper-panels; black dashed lines denote rest posture). Plots show the position trajectory of tongue tip (lower-left panel; dashed lines denote target trajectory) and the predicted muscle activations for simulated upward-bending (lower-right panel).

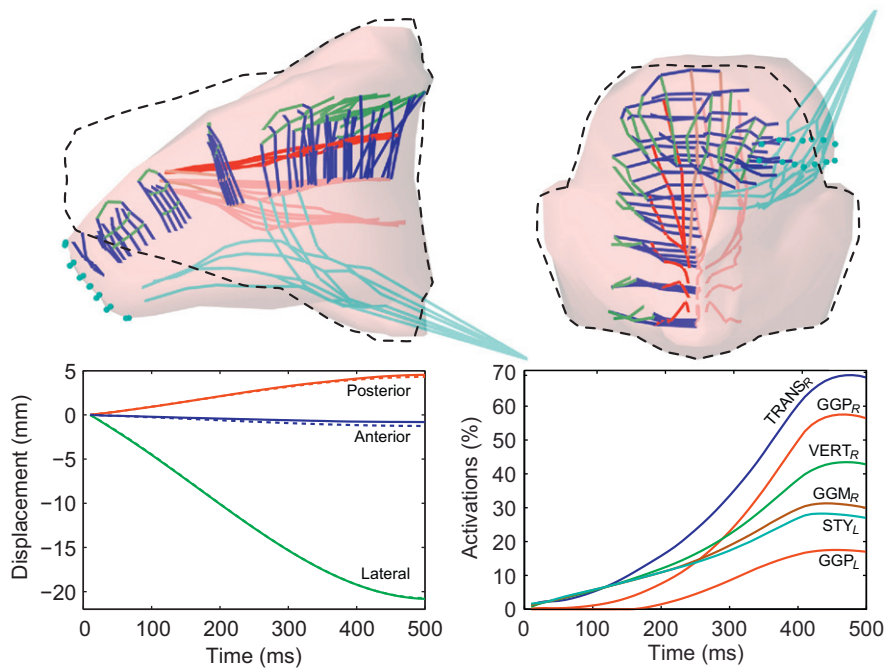


Fig. 6. Top and front views of the tongue model in the final laterally bended posture (upper-panels; black dashed lines denote rest posture). Plots show the position trajectory of tongue tip (lower-left panel; dashed lines denote target trajectory) and the predicted muscle activations for simulated left-sided bending (lower-right panel).

simulations (e.g. the forward-dynamics simulation was only 10 times slower than real-time). Our other assumptions include: attachment locations for muscles, muscle force generating capacity per unit physiological cross-sectional area, and the passive material properties of tongue tissue based on ex vivo measurements (Gerard et al., 2005). MR elastography has recently been used to

measure tongue tissue mechanical properties in vivo (Cheng et al., 2011b). Also, diffusion-tensor MRI shows promise for eliciting detailed data on muscle fiber architecture in the tongue (Gilbert et al., 2006). These advanced MRI-based measurements could potentially be used to better calibrate the location, physiological cross-sectional area, fiber directions, and

mechanical properties of muscles in a future high-fidelity subject specific tongue model.

Our model incorporates muscle mechanics with Hill-type muscle fiber elements. A more detailed distribution of muscle stress would require an active muscle stress term in the constitutive equation of the FE material, such as in the muscle model by Blemker et al. (2005). A more detailed analysis of tongue's myoarchitecture would require a multiscale conceptualization of tongue muscle mechanics, such as in the approach by Mijailovich et al. (2010). Our current muscle model includes the active force-length properties of muscle and relative muscle strengths derived from physiological cross-sectional area measurements. Therefore, we are confident that the relative contributions of the muscle activations predicted with our technique are plausible. Our tracking-based controller is sufficiently general to be used with more sophisticated FE-based muscle models, which is planned as future work.

Despite these limitations, a pertinent factor is that our model represents the tongue in 3D. Since the mechanical support is attributed to volume-preservation in muscular-hydrostat models, it follows that 3D models are required to accurately represent the volumetric aspects of muscular-hydrostat movement. A 2D analysis, as first proposed by Kier and Smith (1985), illustrates the effect of longitudinal muscle forces in bending, but is insufficient to capture volumetric effects. Only by employing a 3D analysis, were we able to illustrate how contralateral transverse muscle forces contribute to lateral tongue bending.

4.2. Comparison with electromyography

Previous studies using tracking-based simulation to predict muscle activations in musculoskeletal systems have compared their results to electromyographic recordings of limb muscles (Thelen and Anderson, 2006; Hamner et al., 2010). Fine-wire electromyography of the tongue is more challenging than surface electromyography of limb muscles, because of the inter-digitation of fibers from different muscles and wire movement during tongue deformation. However, a recent study has reported electromyographic and single-unit recordings during tongue protrusion (Pittman and Bailey, 2009). Our predicted muscle activations during simulated unimpeded tongue protrusion were consistent with these electromyographic recordings showing that both extrinsic (genioglossus) and intrinsic (transverse and vertical) tongue muscles were recruited.

4.3. Comparison with tagged MRI strains

Tagged MRI measurements of tissue strain have been reported for static tongue postures (Napadow et al., 1999) as well as repeated tongue movements in speech (Parthasarathy et al., 2007). The muscle stresses that give rise to observed tissue strains however are not directly measured and must be interpreted from the strain data. For this reason, forward-dynamics simulations with FE models provide a complementary approach to tagged MRI, by directly estimating the effect of muscle stresses to produce tissue strains.

Our simulation results are qualitatively consistent with the tongue strain distributions reported by Napadow et al. (1999). For anterior protrusion, strain was observed within the tongue body (see Napadow et al., 1999, Fig. 2), which is consistent with our predicted recruitment of bilateral intrinsic muscles. For upward bending, strain was observed along the upper tongue surface (see Napadow et al., 1999, Fig. 1) consistent with our predicted superior longitudinal recruitment. Strain was also observed throughout the lower tongue body consistent with our predicted transverse and mylohyoid muscle recruitment. For lateral bending, strain was observed in the contralateral tongue body (see Napadow et al., 1999, Fig. 3) consistent with our predicted contralateral intrinsic and genioglossus muscle

recruitment. Napadow et al. suggested that the contralateral muscle activation stiffened the tongue to enhance the bending effect of ipsilateral longitudinal muscle activation. Our results suggest a stronger contribution of contralateral muscle activation to cause unilateral protrusion of the tongue and bending toward the ipsilateral side.

4.4. Lateral tongue bending

The simulation results support our hypothesis that contralateral transversely oriented tongue muscles would be required in addition to the ipsilateral portion of the superior longitudinal muscle in lateral tongue bending. For upward tongue bending, recruitment of the superior longitudinal muscle alone was sufficient, which is consistent with the muscular-hydrostat theory proposed by Kier and Smith (1985). However, for lateral bending the lateral portions of the superior longitudinal muscle in the tongue were too small to generate sufficient force to produce significant lateral tongue bending and therefore the contralateral muscles were also recruited. This auxiliary mechanism of bending – synergistic activation of ipsilateral longitudinal fibers and contralateral transverse and vertical fibers – is diagrammed in Fig. 7 for an idealized muscular-hydrostat beam.

The relationship between contralateral muscle activation and lateral tongue bending can also be observed in unilateral stroke patients. Unilateral stroke commonly results in lateral deviation of the tongue toward the side of limb weakness during attempted tongue protrusion (Umaphathi et al., 2000). The deviation is caused by unilateral activation of contralateral protrusion tongue muscles (genioglossus and intrinsic muscles) due to paralysis of the ipsilateral muscles. During lateral-bending, tongue muscles on the contralateral side can be thought of as pushing the tongue toward the opposite side due to hydrostatic effects. Interestingly, lateral deviation of the jaw is also generated by contralateral muscle recruitment, namely, the lateral pterygoid muscle in the case of the jaw (Murray et al., 2007).

4.5. Muscle redundancy

Muscle redundancy in biomechanical systems prevents muscle activations from being uniquely predicted by inverse analysis techniques. Muscle redundancy is observed in our predictions of synergistic recruitment of extrinsic and intrinsic tongue muscles for protrusion. In our current simulations, muscle redundancy was resolved with a regularization term in the optimization that minimized the sum-square of muscle activations. This is a common assumption in static-optimization studies (Erdemir et al., 2007) and has been shown to be effective for predicting muscle excitations that match electromyography in gait with healthy subjects (Hamner et al., 2010).

In the tongue, redundancy between extrinsic and intrinsic muscles may also be resolved by auxiliary biomechanical factors, such as tissue stiffness caused by co-activation of orthogonally arranged muscle fibers. Interestingly, intrinsic muscle activity alone, and not genioglossus muscle activity, increases during tongue protrusion against an external obstruction (Pittman and Bailey, 2009), which suggests a simultaneous increase in tongue stiffness. We are currently extending our forward-dynamics tracking method to include stiffness targets in addition to movement targets, which could be used to systematically investigate the role of stiffness in resolving tongue muscle redundancy.

4.6. Simulation methods

Our current analysis used nodes at the tongue tip to characterize the target movement. Our simulation framework permits the use of

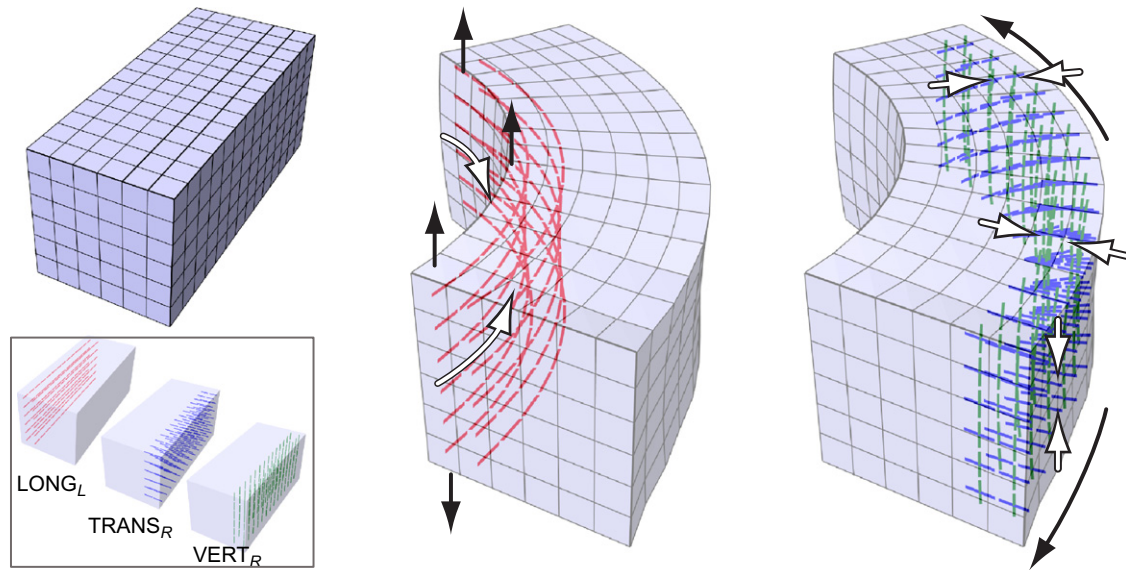


Fig. 7. Mechanisms of lateral bending in an idealized muscular-hydrostat model (left image; shown at rest) with orthogonal muscle fibers (inset). The direction of muscle forces are illustrated with white arrows and the direction of resulting movement with black arrows. Lateral longitudinal muscle forces caused lateral longitudinal compression and lateral vertical expansion (center image). Contra-lateral vertical muscle forces caused contralateral vertical compression and contralateral longitudinal expansion (right image). Both lateral longitudinal compression and contralateral longitudinal expansion contributed to lateral bending.

any type of target movement, so long as it can be characterized as a linear combination of the model's degrees-of-freedom. Biomechanical variables other than movement could also be used as targets in our formulation. These variables could include tissue stiffness as well as tongue-palate contact pressure (Ono et al., 2009). Contact pressure targets have been used in a previous study with a rigid-body jaw model to control bite force (Stavness et al., 2010).

We have reported a qualitative comparison of muscle activations predicted by our simulations and muscle activations interpreted from tagged-MRI data. Our analysis technique could also be used to perform quantitative comparisons of tissue strain, however such a study would require a high-fidelity subject-matched tongue model. This type of quantitative analysis with a detailed model has been reported for 2D simulations of mid-sagittal tongue deformations during swallowing (Mijailovich et al., 2010). Within our framework for 3D FE simulations, a quantitative comparison would use tagged MRI to directly specify boundary conditions and target motion for the inverse FE simulation. The resulting internal tissue strains predicted by the simulation would be quantitatively compared to the tissue strains derived from tagged MRI data.

Although the present study has focused on muscular-hydrostat systems, our simulation framework is generally applicable to coupled hard-soft tissue musculoskeletal systems (Stavness et al., 2011). This permits a similar automatic analysis of muscle forces in high-fidelity limb models that combine rigid bone structures with detailed 3D FE models of skeletal muscles (Blemker and Delp, 2005). For such models, the target movement would be experimentally recorded skeletal kinematics, while the simulation output would be muscle stress distributions.

4.7. Potential clinical applications

The simulation techniques applied here could be used to analyze the functional consequences of altered tongue morphology, such as that after glossectomy and free-flap tongue reconstruction (Bressmann et al., 2007; Stone and Murano, 2007). Surgery can result in dramatic changes to tongue structure, including removal of tongue muscles, addition of grafted tissue, and change in tissue stiffness due to scarring. We have previously investigated compensatory muscle

forces consequent to mandibular resection (Stavness et al., 2010) using forward-dynamics tracking simulation with a rigid-body jaw model. A similar approach could be employed to predict compensatory tongue muscle forces and guide post-operative therapy following glossectomy.

Another relevant clinical application of our analysis technique is the pathophysiology of obstructive sleep apnea (OSA). OSA involves constriction of the airway during sleep and its cause has been attributed to a number of separate biomechanical factors, including air pressure, tissue compliance (Schwab, 2003), and muscle activity (Schwartz et al., 2008). Our inverse simulation technique could be used in combination with reported measurements of genioglossus electromyography (Malhotra et al., 2002) and tagged MRI of the tongue (Cheng et al., 2011a) to predict the muscle forces that contribute to tongue root motion during breathing, given the boundary conditions and air pressure forces imparted on the tongue.

To summarize, we have demonstrated a forward-dynamics tracking simulation for automatically predicting muscle recruitment patterns to perform protrusion and bending movements with an FE tongue model. The resulting simulated tongue deformations were consistent with published data on tongue strain during matched tongue movements. Moreover, the predicted muscle activation patterns provide a theoretical proposal for how muscle forces contribute to observed tongue strain. Our tracking-based controller, forward-dynamics simulator, and FE tongue model are open-source and freely available for download with the ArtiSynth modeling toolkit at www.artisynth.org.

Conflict of interest statement

None of the authors have any conflict of interest with regard to this study.

Acknowledgments

This work was supported by the Natural Sciences and Engineering Research Council of Canada. The authors thank Gipsa-Lab, Grenoble

for the tongue model geometry (S. Buchaillard, J.M. Gérard, P. Perrier, Y. Payan).

Appendix A. Supplementary material

Supplementary data associated with this article can be found in the online version of <http://dx.doi.org/10.1016/j.jbiomech.2012.08.031>.

References

- Blemker, S., Delp, S., 2005. Three-dimensional representation of complex muscle architectures and geometries. *Annals of Biomedical Engineering* 33 (5), 661–673.
- Blemker, S., Pinsky, P., Delp, S., 2005. A 3D model of muscle reveals the causes of nonuniform strains in the biceps brachii. *Journal of Biomechanics* 38 (4), 657–665.
- Bressmann, T., Ackloo, E., Heng, C., Irish, J., 2007. Quantitative three-dimensional ultrasound imaging of partially resected tongues. *Otolaryngology—Head and Neck Surgery* 136 (5), 799–805.
- Buchaillard, S., Perrier, P., Payan, Y., 2009. A biomechanical model of cardinal vowel production: muscle activations and the impact of gravity on tongue positioning. *Journal of the Acoustical Society of America* 126 (4), 2033–2051.
- Cheng, S., Butler, J., Gandevia, S., Bilston, L., 2011a. Movement of the human upper airway during inspiration with and without inspiratory resistive loading. *Journal of Applied Physiology* 110 (1), 69–75.
- Cheng, S., Gandevia, S., Green, M., Sinkus, R., Bilston, L., 2011b. Viscoelastic properties of the tongue and soft palate using mr elastography. *Journal of Biomechanics* 44 (3), 450–454.
- Erdemir, A., McLean, S., Herzog, W., van den Bogert, A.J., 2007. Model-based estimation of muscle forces exerted during movements. *Clinical Biomechanics* 22 (2), 131–154.
- Fang, Q., Fujita, S., Lu, X., Dang, J., 2009. A model-based investigation of activations of the tongue muscles in vowel production. *Acoustical Science and Technology* 30 (4), 277–287.
- Gerard, J.M., Ohayon, J., Luboz, V., Perrier, P., Payan, Y., 2005. Non linear elastic properties of the lingual and facial tissues assessed by indentation technique: application to the biomechanics of speech production. *Medical Engineering & Physics* 27 (10), 884–892.
- Gilbert, R., Napadow, V., Gaige, T., Wedeen, V., 2007. Anatomical basis of lingual hydrostatic deformation. *Journal of Experimental Biology* 210 (23), 4069.
- Gilbert, R.J., Magnusson, L.H., Napadow, V.J., Benner, T., Wang, R., Wedeen, V.J., 2006. Mapping complex myoarchitecture in the bovine tongue with diffusion-spectrum magnetic resonance imaging. *Biophysical Journal* 91 (3), 1014.
- Hamner, S.R., Seth, A., Delp, S.L., 2010. Muscle contributions to propulsion and support during running. *Journal of Biomechanics* 43 (14), 2709–2716.
- Hughes, T.J.R., 2000. *The Finite Element Method: Linear Static and Dynamic Finite Element Analysis*. Dover Publications, New York.
- Kier, W.M., Smith, K.K., 1985. Tongues, tentacles and trunks: the biomechanics of movement in muscular-hydrostats. *Zoological Journal of the Linnean Society* 83 (4), 307–324.
- Liang, Y., McMeeking, R., Evans, A., 2006. A finite element simulation scheme for biological muscular hydrostats. *Journal of Theoretical Biology* 242 (1), 142–150.
- Lloyd, J.E., Stavness, I., Fels, S. Artistry: a fast interactive biomechanical modeling toolkit combining multibody and finite element simulation. In: Payan, Y. (Ed.), *Soft Tissue Biomechanical Modeling for Computer Assisted Surgery*, studies in Mechanobiology, Tissue Engineering and Biomaterials. vol. 11. Springer Berlin Heidelberg, pp. 355–394. ISBN: 978-3-642-29014-5, http://dx.doi.org/10.1007/8415_2012_126.
- Malhotra, A., Pillar, G., Fogel, R., Edwards, J., Ayas, N., Akahoshi, T., Hess, D., White, D., 2002. Pharyngeal pressure and flow effects on genioglossus activation in normal subjects. *American Journal of Respiratory and Critical Care Medicine* 165 (1), 71–77.
- Mijailovich, S., Stojanovic, B., Kojic, M., Liang, A., Wedeen, V., Gilbert, R., 2010. Derivation of a finite-element model of lingual deformation during swallowing from the mechanics of mesoscale myofiber tracts obtained by mri. *Journal of Applied Physiology* 109 (5), 1500.
- Murray, G.M., Bhutada, M., Peck, C.C., Phanachet, I., Sae-Lee, D., Whittle, T., 2007. The human lateral pterygoid muscle. *Archives of Oral Biology* 52 (4), 377–380.
- Napadow, V., Chen, Q., Wedeen, V., Gilbert, R., 1999. Intramuscular mechanics of the human tongue in association with physiological deformations. *Journal of Biomechanics* 32 (1), 1–12.
- Ono, T., Hori, K., Tamine, K., Maeda, Y., 2009. Evaluation of tongue motor biomechanics during swallowing—from oral feeding models to quantitative sensing methods. *Japanese Dental Science Review* 45 (2), 65–74.
- Pai, D.K., 2010. Muscle mass in musculoskeletal models. *Journal of Biomechanics* 43 (11), 2093–2098.
- Parthasarathy, V., Prince, J.L., Stone, M., Murano, E.Z., NessAiver, M., 2007. Measuring tongue motion from tagged cine-MRI using harmonic phase (HARP) processing. *Journal of the Acoustical Society of America* 121, 491.
- Pittman, L.J., Bailey, E.F., 2009. Genioglossus and intrinsic electromyographic activities in impeded and unimpeded protrusion tasks. *Journal of Neurophysiology* 101 (1), 276.
- Schwab, R., 2003. Pro: sleep apnea is an anatomic disorder. *American Journal of Respiratory and Critical Care Medicine* 168 (3), 270–271.
- Schwartz, A., Patil, S., Laffan, A., Polotsky, V., Schneider, H., Smith, P., 2008. Obesity and obstructive sleep apnea pathogenic mechanisms and therapeutic approaches. *Proceedings of the American Thoracic Society* 5 (2), 185–192.
- Sifakis, E., Neverov, I., Fedkiw, R., 2005. Automatic determination of facial muscle activations from sparse motion capture marker data. *ACM Transactions on Graphics* 24 (July (3)), 417–425.
- Stavness, I., Hannam, A.G., Lloyd, J., Fels, S., 2010. Predicting muscle patterns for hemimandibulectomy models. *Computer Methods in Biomechanics and Biomedical Engineering* 13 (4), 483–491.
- Stavness, I., Lloyd, J., Payan, Y., Fels, S., 2011. Coupled hard–soft tissue simulation with contact and constraints applied to jaw–tongue–hyoid dynamics. *International Journal of Numerical Methods in Biomedical Engineering* 27 (3), 367–390.
- Stone, M., Murano, E., 2007. Speech patterns in a muscular hydrostat: normal and glossectomy tongue movement. In: *Proceedings of the International Symposium on Biomechanics, Healthcare and Information Science*, pp. 163–170.
- Sueda, S., Kaufman, A., Pai, D.K., 2008. Musculotendon simulation for hand animation. In: *ACM SIGGRAPH Papers*, pp. 1–8.
- Thelen, D.G., Anderson, F.C., 2006. Using computed muscle control to generate forward dynamic simulations of human walking from experimental data. *Journal of Biomechanics* 39 (6), 1107–1115.
- Umapathi, T., Venketasubramanian, N., Leck, K., Tan, C., Lee, W., Tjia, H., 2000. Tongue deviation in acute ischaemic stroke: a study of supranuclear twelfth cranial nerve palsy in 300 stroke patients. *Cerebrovascular Diseases* 10 (6), 462–465.
- Wang, Y., Röhrle, O., Nielsen, P., Pullan, A., Kieser, J., Nash, M., July 2011. Investigating muscle co-activation during tongue elongation using an anatomically-based finite element model of the tongue. In: *23rd International Society of Biomechanics Congress (ISB)*, No. 797 (online).
- Wilhelms-Tricarico, R., 1995. Physiological modeling of speech production: methods for modeling soft-tissue articulators. *Journal of the Acoustical Society of America* 97, 3085–3098.
- Yekutieli, Y., Sagiv-Zohar, R., Aharonov, R., Engel, Y., Hochner, B., Flash, T., 2005. Dynamic model of the octopus arm. I. Biomechanics of the octopus reaching movement. *Journal of Neurophysiology* 94 (2), 1443.
- Zajac, F., 1989. Muscle and tendon: properties, models, scaling, and application to biomechanics and motor control. *Critical Reviews in Biomedical Engineering* 17 (4), 359.